

High Resolution Tunnelling Spectroscopy of a Graphene Quartet

Young Jae Song^{1,2}, Alexander F. Otte^{1,2}, Young Kuk^{1,§}, Yike Hu³, David B. Torrance³, Phillip N. First³, Walt A. de Heer³, Hongki Min^{1,2}, Shaffique Adam¹, Mark D. Stiles¹, Allan H. MacDonald⁴, and Joseph A. Stroscio^{1,*}

¹*Center for Nanoscale Science and Technology, NIST, Gaithersburg, MD 20899*

²*Maryland NanoCenter, University of Maryland, College Park, Maryland 20742*

³*School of Physics, Georgia Institute of Technology, Atlanta, GA 30332*

⁴*Department of Physics, University of Texas at Austin, Austin, TX 78712*

Electrons in the graphene 2D electron system behave quite differently from those in traditional 2D electron systems. Like massless relativistic particles, they have linear dispersion and chiral eigenstates. In addition, there are two sets of electrons centred at different points in reciprocal space (valleys) that have this dispersion, giving rise to valley degeneracy. The symmetry between valleys, together with spin symmetry, leads to a four-fold *quartet* degeneracy of the Landau levels - peaks in the density of states produced by an applied magnetic field. Recent electron transport measurements have observed the lifting of the four-fold degeneracy in very large applied magnetic fields separating the quartet into integer¹⁻⁴, and more recently into fractional^{5,6}, levels. The exact nature of the broken-symmetry states that form within the Landau levels and lift these degeneracies is unclear at present

[§] Permanent address: Department of Physics, Seoul National University, Seoul, Korea

* Corresponding author, email: joseph.stroscio@nist.gov

and a topic of intense theoretical debate⁷⁻¹¹. Here we report on the direct observation of the behaviour of the four quantum states that make up a degenerate graphene Landau level. We use high resolution scanning tunnelling spectroscopy in an applied magnetic field to study the top-layer of multi-layer epitaxial graphene. When the Fermi level lies inside the four-fold Landau manifold, significant electron correlation effects result in an enhanced valley splitting at even filling factors, and an enhanced electron spin splitting at odd filling factors. Most surprisingly, we observe states with Landau level filling factors 7/2, 9/2, and 11/2, suggestive of new many body states in graphene.

When matter is put under extreme conditions, it often exhibits new quantum phases; examples include superconductivity¹², the integer quantum Hall effect¹³, and the fractional quantum Hall effect¹⁴. The history of fractional quantum Hall states in semiconductor hetero-junctions suggests that studying graphene at lower temperatures and higher magnetic fields will also reveal new quantum phases of matter. The phases of two-dimensional electron systems (2DES) in semiconductor quantum wells are most commonly probed by electron transport measurements. On the other hand, tunnelling spectroscopy, which has long been recognized as a powerful probe of 2D electron systems, has been difficult to apply to the buried 2DES's in semiconductor quantum wells. Fortunately, graphene 2DES's are located on the surface of the material and quantum Hall physics can be studied now that instruments are available that work at the necessary temperatures and fields. Recent scanning tunnelling spectroscopy (STS) measurements in an external magnetic field B have verified the expected magnetic quantization relation in epitaxial graphene layers grown on SiC¹⁵, with Landau level energies given by $E_N = \text{sgn}(N)c^*\sqrt{2e\hbar B|N|}$, where $N = 0, \pm 1, \pm 2, \dots$ is the orbital quantum index, c^* is the graphene dispersion velocity, and \hbar is Planck's constant divided by 2π . In the current work, we achieve much higher energy resolution with a scanning probe microscope system operating at temperatures T as low as 10 mK in

magnetic fields up to 15 T (see methods). These are the lowest temperatures achieved in any scanning tunnelling microscope and yield spectroscopic resolution ($\approx 3k_B T$) that is orders of magnitude better than previous measurements of graphene by STS at 4 K^{15,16}. Recent spectroscopic measurements of the density of states in 2D electron systems¹⁷, which have similar resolution, have observed electron correlation effects in quantum well systems. The present measurements resolve spectroscopic features that suggest new many body quantum states also occur under these extreme conditions in epitaxial graphene.

The growth of epitaxial graphene (Fig. 1, upper left inset) on the carbon-face of SiC results in a multilayer film with rotational misalignment between the layers^{18,19}, leading to moiré interference patterns in scanning tunnelling microscopy (STM) images (Supplementary Fig. 1)^{15,20}. The visible moiré unit cell dimension determines the rotational angle between the top two layers²⁰. We measure a unit cell length of 5.7 nm (Supplementary Fig. 1) and hence a rotation angle of 2.3°. The small angle rotation reduces the interlayer coupling resulting in layers that have electrical properties nearly identical to a single-graphene-layer^{15,18}. This single-layer-like behaviour is confirmed by the orbital Landau quantization measured by STS (Fig. 1), which shows excellent single layer graphene scaling with carrier velocities $\approx 10^6$ ms⁻¹ (Fig. 1, upper right inset). In Fig. 1, the $N=0$ LL (E_0) is located at -134 mV, which is close to the zero field Dirac point (E_D) of -125 mV corresponding to an *n*-type doping of 1×10^{12} cm⁻² (Supplementary Fig. 2). Note that the magnetic oscillation intensity drops smoothly with energy difference from the Fermi energy. This envelope may be related to quasiparticle lifetimes, which decrease with the energy difference from E_F . We do not observe any LLs with negative orbital index N , presumably due to this envelope.

We first concentrate on the field dependence of the LLs with large energy range measurements. Figure 2 shows the evolution of the LL series as a function of magnetic

field. Each panel of the indicated field consists of 21 dI/dV spectra acquired at different spatial points along a line (the same for each panel) of 40 nm. The horizontal axis for all panels is the sample bias voltage, and the vertical axis in each panel indicates the position along the line where the spectrum was acquired; the resulting dI/dV intensity is shown in a colour scale. In this way the LLs appear as a spectral fingerprint; one can see the reproducibility of the spectra and their evolution with magnetic field. In particular the lower LL_N (for example the ones labelled $N=0, 1$, and 2) are easily seen and can be tracked visually as the magnetic field is varied (Fig. 2). In addition, there are a number of non-Landau level related peaks when LL_1 crosses E_F at zero sample bias between 11 T and 14 T. These additional states (which appear in groups of four) vary with spatial position and magnetic field much more than the LLs themselves. Other sets of these peaks are seen weakly when LL_2 crosses E_F at 5 T. Analysis of these non-Landau level peaks is beyond the scope of the present article.

We can make several important observations from these spectral prints. The position of LL_0 in Fig. 2 shows reproducible steps in its energy position as a function of magnetic field, in particular, between 7 T and 8 T, and 11 T to 12 T. For an isolated graphene sheet, the position of the $N=0$ Landau level should be fixed at the Dirac charge neutrality point E_D , and should not depend on the magnetic field. However, as seen in Fig. 2, the position of the LL_0 peak shifts to lower energy with increasing magnetic field. This shift coincides with a shift of the other Landau levels as well, so that the spectra preserve the scaling relation with magnetic field as indicated in Fig. 1. The density of electrons in the top layer is easily calculable when all Landau levels are filled or empty, $n=vB/\Phi_0$, where v is the filling factor (where we count two levels for $N=0$ plus four each for $N>0$) and Φ_0 is the flux quantum. Figure 3a shows that this density varies by almost a factor of two as the field is swept. This variation indicates that charge is transferred between the top layer and layers below. Such transfers arise because the magnetic field changes the densities of states in the carbon sheets below the

top-most layer, in turn changing the energy balance between the single particle energies and the electrostatic potential. This competition apparently drives the charge flow between the layers to keep the Landau levels in the top layer either filled or empty. Even though the charge density in the top layer is not fixed, there is still a tendency for the filling-factor to decrease with field.

A close examination of the $N=0$ to $N=2$ LLs reveals a remarkable pattern of splittings (Fig. 2). The $N=1$ and $N=2$ LL splitting is clear at lower fields, while the $N=0$ splitting is more visible above 12 T because of the broadening of this level at the higher energy. We associate the largest splittings we observe to broken valley degeneracy, by examining LL_1 in high resolution measurements. The Landau levels split into a *quartet* at higher applied fields (Fig. 4). Figure 4a shows a series of dI/dV line scans, obtained in the same spatial locations as in Fig. 2 with ten times higher energy resolution, which reveal reorganizations of the LL_1 density-of-states as it crosses through the Fermi level for magnetic fields from 11 T to 12 T. Figure 4b shows representative line spectra for each magnetic field extracted from Fig. 4a. Starting at the lowest panel in Fig. 4a (at 11 T), the four peaks (bright lines) correspond to the four-fold manifold of LL_1 . The four separate peaks in Fig. 4b at 11 T reveal a LL_1 quartet in which both spin and valley degeneracies are lifted. Figure 5a, upper inset, shows a schematic of the energy level structure of the $N=1$ LL. The electron spin up and down levels are indicated by the up and down arrows. This assignment is confirmed by more detailed measurements as a function of field described below.

The spectrum at 11 T (the bottom panel in Figs. 4a,b) shows all four peaks clearly below E_F indicating a filling factor $v=6$ (two filled levels for $N=0$ plus four for $N=1$). Focusing on the 3rd panel from the bottom at 11.25 T in Fig. 4a and 4b, the Fermi-level is located between the right two spin-split levels of LL_1 , leading to a polarized state at a filling factor $v=5$ and a greatly enhanced spin splitting due to a strong exchange

interaction. Very interestingly, at the lower magnetic field of 11.125 T (2nd panel from the bottom) a new peak appears in LL₁, making a three-fold LL spin sub-manifold. An examination of the spectra shows that the intensity of the right-most two peaks on either side of E_F are $\frac{1}{2}$ the intensity of the 3rd spin up peak of that sub-manifold. Thus the original spin-down feature splits into two spin-down peaks with $\frac{1}{2}$ the intensity on either side of E_F . This state corresponds to a new stable quantum state with a top-layer filling factor of $v=11/2$. Progressing to higher fields as we go up vertically in the series (Figs. 4a,b), we see again another stable $\frac{1}{2}$ -filled state at $v=9/2$ just before both spin split states empty and go above E_F at 11.625 T at $v=4$. Finally, a 3rd $\frac{1}{2}$ -filled state is observed at higher fields (14 T) when E_F is now in the left set of the spin split states at a filling factor of $v=7/2$. An examination of fine field adjustments shows that these $\frac{1}{2}$ -filled quantum states are the only stable states that are observed between the $v=4$ and $v=6$ states (Figs. 3b,c). Figure 3b shows the integrated intensity of the dI/dV spectra for the filled states of the K' valley (rightmost valley peaks) from the midpoint of the $N=1$ LL to the Fermi level (zero bias). As each LL empties, the integrated intensity jumps down to a new plateau that is stable over a finite field range. The size of each jump in Fig. 3b corresponds to one-half the intensity of single LL, demonstrating these are stable $\frac{1}{2}$ -filled states. Normalizing the integrated intensity to a single LL (*i.e.* value at $v=5$) yields filling factors of 5.46 ± 0.06 and 4.54 ± 0.04 (error is one standard deviation, 1σ) between $v=6$ to $v=5$, and $v=5$ to $v=4$, respectively. The energy separation between $\frac{1}{2}$ -fractional LLs ranges from 3 meV at $v=11/2$ to about 5.5 meV at $v=7/2$ at 14 T.

Earlier transport measurements^{1,2} at filling factors of 0 and ± 1 observed the lifting of the level degeneracies and initially interpreted the results as demonstrating the lifting of the spin degeneracy followed by the lifting of valley degeneracy for LL₀. States at a filling factor of ± 4 were also observed¹ and tentatively ascribed to the lifting of the spin degeneracy for LL₁. In Figs. 5a,b, we plot the energy separations between spectral peak positions in the LL₁ manifold in Fig. 4 to determine their origin. We identify the larger

energy splitting as arising from the lifting of the valley degeneracies because the g-factors of the smaller splitting are close to 2, as expected for electron spins. The larger energy splitting observed in LL₁ is also observed in LL₀ and LL₂ (Fig. 2) in a limited range of magnetic fields. For LL₁ the energy splitting is about ten times the value of the Zeeman energy for electron spin ($g\mu_BB$). A fitting of the linear portion of the valley energy splitting yields an effective g-factors of $g_V(LL_1) = 18.4 \pm 0.4$ (1σ). Interestingly, the valley splitting is enhanced in LL₁ as E_F becomes centred in the LL₁ (Fig. 4) at a filling factor of $\nu=4$, which gives rise to a peak in the splitting energy versus field (Fig. 5a). Figure 5b shows the various energy separations between the spin up and down LLs of the same valley polarization. The separations between the left and right valley polarized levels are shown in red and blue symbols, respectively, and differ slightly by approximately 5 %. A linear fit yields g-factors of $g_{SL} = 2.36 \pm 0.01$ and $g_{SR} = 2.23 \pm 0.01$ (1σ). An enhancement is observed in the spin split states when they become polarized at odd filling (filling factor $\nu=5$ in Fig. 4 and orange symbols Fig. 5b). This enhancement is a factor of three greater than normal Zeeman splitting and is driven by the exchange interaction of the fully polarized spin level similar to exchange enhancements observed in Si 2D electron systems²¹, and later investigated in GaAs 2D systems^{22,23}. For graphene, we expect a different enhancement since the screening and dielectric properties are significantly different than in semiconductor 2D electron systems.

In graphene systems with weak disorder, interaction driven gaps are expected⁷ to lift Landau level degeneracies. This epitaxial graphene sample is in the weak disorder limit where interaction physics is expected to dominate based on the observed LL linewidths of the order of 0.5 meV. Although we do not have a complete explanation for all the effects we observe, particularly those at fractional top-layer filling factors, we highlight some considerations that are likely to be important.

The LL_1 valley splitting varies non-linearly with field above 7 T. We believe that the valley splitting is due in part to single-electron inter-layer coupling effects which are sensitive to the energies of submerged levels, and in part to enhancement by interactions. The valley splitting displays a sharp peak at 12 T when E_F is exactly centred in LL_1 corresponding to the filling factor of 4. This enhancement suggests that electron correlations enhance the valley splitting at $\nu=4$.

Over the field range between 10 T and 14 T the $N=1$ Landau level of the top layer progressively empties. The filling factor ν is not inversely proportional to field, but decreases via a sequence of jumps corresponding to first order phase transitions between especially stable states (see Fig. 3b,c). In particular, we observe surprising new states in which the top-layer, spin- and valley-split Landau level at the Fermi energy splits further into separate occupied and empty contributions. Viewing the tunnelling spectra as a correlated-state fingerprint, we determine that the state with these spectral features is stable over a finite range of applied field, giving way to even and odd filling factor states at the extremes of its stability range (Figs. 3c and 4). Since the integrated intensity of the two smaller spectral features is half the intensity of the major peak (Fig. 3b), the new quantum states occur with top-layer filling factors $\nu=11/2$, $9/2$, and $7/2$. The abrupt field-dependence of the density-of-states signals a first order phase transition between electronic states with qualitatively different electronic correlations. Interaction induced gaps within a Landau level, like the ones we have observed, frequently signal interesting new physics. An example is the fractional quantum Hall effect, which has recently been observed in high mobility suspended graphene samples at $\nu=1/3^{5,6}$. Our experimental observations suggest that electron-electron interactions are responsible for especially stable states of $N=1$ graphene electrons with top-layer filling factors close to odd integers and half-odd-integers. Although further experiments may be necessary to clarify the physics of the $N=1$ half-filled Landau level states, the following considerations provide some guidance.

The top-layer that we probe is in close proximity to five buried layers that influence top-layer physics not only by serving as a charge reservoir, but also by screening interactions between top-layer electrons. The screening by the buried layers can be described crudely by modelling them as an effective metallic screening layer that is separated from the top layer by a distance d_{eff} , which should be smaller than the total thickness of the carbon layer, *i.e.* less than around 2 nm. Since d_{eff} is smaller than the magnetic length $l_B \approx 10$ nm, the Coulomb interaction of electrons in the top layer are screened for distances larger than d_{eff} giving an effective short-range interaction potential $V_0 = 4\pi e^2 d_{\text{eff}} / \epsilon$, where ϵ accounts crudely for screening effects within the top layer due to both inter Landau-level and σ bond polarization and dielectric screening by the SiC substrate. Short range repulsive interactions favour spin-polarized states at odd integer filling factors and contribute an exchange-correlation contribution

$$\Delta_{\text{XC}} = n_{\text{LL}} V_0 = 2e^2 d_{\text{eff}} / \epsilon l_B^2$$

to the gap between majority and minority spin levels^{21,22}.

This approximate expression yields values consistent with the experimentally observed gap between majority and minority spin levels at filling factor $v=5$ (Fig. 5b).

A number of possibilities come to mind for the gaps at fractional top layer fillings. They could, for example, be associated with the formation of charge density wave states^{24,25}, like those that occur in semiconductor quantum wells when $N > 0$ Landau levels are partially filled^{26,27}, or to the exotic $S=N/2$ or $S=0$ states suspected as the origin of the $N=1$, $v=5/2$ quantum Hall effects in semiconductors.²⁸ An alternate explanation, however, is suggested by the surprisingly large value of the fractional gap relative to the enhanced spin-splitting. In multi-layer systems stable states can form at fractional filling factor per layer by forming counter-flow superfluid states with spontaneous interlayer coherence²⁹. The fractional state gap-size Δ_f would then be proportional to the inter-layer interaction strength, which in our system should be nearly as large as Δ_{XC} because of the close proximity between different layers. Experimentally we find $\Delta_f \approx \Delta_{\text{XC}}$ in agreement with this hypothesis.

Our observations suggest a number of future experiments. The ability to gate the graphene/SiC system and change the filling factor at fixed field would allow more magnetic quantum levels to be placed at the Fermi-level, in particular, the $N=0$ LL, where 1/3 fractional quantum states should be observed in the tunnelling density of states¹⁷. We expect that, as in the semiconductor case, different correlated states will be revealed when LLs with different N are pushed to the Fermi energy. In addition, the spatial variation of the Landau levels is likely to be rich because the zero field energy scale of the disorder potential is of the same order as the splitting energies of the Landau levels. In the future, we expect that ultralow temperature high field scanning probe microscopy will continue to reveal new physics related to the electronic structure of graphene.

Methods

The experiments were performed using a newly commissioned ultra-high vacuum (UHV) scanning probe microscope (SPM) facility at NIST that operates with a base temperature of 10 mK and a 15 T magnetic field capability. The epitaxial graphene sample was grown on C-face SiC at the Georgia Institute of Technology using the induction furnace method³⁰. The graphene thickness was estimated to be 6 layers as determined by elliposometry measurements. The sample was transported to NIST in a vacuum suitcase. The sample was introduced through air into the mK SPM system, and subsequently heated in UHV to 200 °C before insertion into the microscope. A Ag tip was prepared by electrochemical etching and subsequent heating and field electron microscopy characterization. All tunnelling measurements were made at temperatures between 13 mK and 20 mK. Temperatures were measured using a superconducting fixed point device, and transferring the temperature scale, via a cerous magnesium nitrate (CMN) susceptibility thermometer, to ruthenium oxide thin film sensors. Tunnelling differential conductance measurements were made using lock-in detection

with a modulation frequency of \approx 500 Hz, and various (root-mean-square) modulation amplitudes depending on the spectral range of interest.

References:

1. Zhang, Y. et al. Landau-Level Splitting in Graphene in High Magnetic Fields. *Physical Review Letters* **96**, 1-4 (2006).
2. Jiang, Z., Zhang, Y., Stormer, H. & Kim, P. Quantum Hall States near the Charge-Neutral Dirac Point in Graphene. *Physical Review Letters* **99**, (2007).
3. Abanin, D.A. et al. Dissipative Quantum Hall Effect in Graphene near the Dirac Point. *Phys. Rev. Lett.* **98**, 196806 (2007).
4. Gusynin, V.P. & Sharapov, S.G. Unconventional Integer Quantum Hall Effect in Graphene. *Phys. Rev. Lett.* **95**, 146801 (2005).
5. Bolotin, K.I., Ghahari, F., Shulman, M.D., Stormer, H.L. & Kim, P. Observation of the fractional quantum Hall effect in graphene. *Nature* **462**, 196-9 (2009).
6. Du, X., Skachko, I., Duerr, F., Luican, A. & Andrei, E.Y. Fractional quantum Hall effect and insulating phase of Dirac electrons in graphene. *Nature* **462**, 192-5 (2009).
7. Nomura, K. & MacDonald, A. Quantum Hall Ferromagnetism in Graphene. *Physical Review Letters* **96**, 256602 (2006).
8. Alicea, J. & Fisher, M. Graphene integer quantum Hall effect in the ferromagnetic and paramagnetic regimes. *Physical Review B* **74**, 75422 (2006).
9. Yang, K., Das Sarma, S. & MacDonald, A. Collective modes and skyrmion excitations in graphene SU(4) quantum Hall ferromagnets. *Physical Review B* **74**, 1-8 (2006).
10. Goerbig, M.O., Moessner, R. & Doucot, B. Electron interactions in graphene in a strong magnetic field. *Phys. Rev. B* **74**, 161407 (2006).
11. Abanin, D., Lee, P. & Levitov, L. Randomness-Induced XY Ordering in a Graphene Quantum Hall Ferromagnet. *Physical Review Letters* **98**, 1-4 (2007).
12. Onnes, H. The resistance of pure mercury at helium temperatures. *Comm. Phys. Lab. Univ. Leiden. No. B* **120**, 3 (1911).
13. Klitzing, K.V., Dorda, G. & Pepper, M. New Method for High-Accuracy Determination of the Fine-Structure Constant Based on Quantized Hall Resistance. *Phys. Rev. Lett.* **45**, 494 (1980).
14. Tsui, D.C., Stormer, H.L. & Gossard, A.C. Two-Dimensional Magnetotransport in the Extreme Quantum Limit. *Phys. Rev. Lett.* **48**, 1559 (1982).
15. Miller, D.L. et al. Observing the quantization of zero mass carriers in graphene. *Science* **324**, 924-7 (2009).
16. Li, G., Luican, A. & Andrei, E. Scanning Tunneling Spectroscopy of Graphene on Graphite. *Physical Review Letters* **102**, 1-4 (2009).
17. Dial, O.E., Ashoori, R.C., Pfeiffer, L.N. & West, K.W. Anomalous structure in the single particle spectrum of the fractional quantum Hall effect. *Nature* **464**, 566-570 (2010).
18. Hass, J. et al. Why Multilayer Graphene on 4H-SiC(0001-bar) Behaves Like a Single Sheet of Graphene. *Phys. Rev. Lett.* **100**, 125504 (2008).
19. Mele, E.J. Commensuration and interlayer coherence in twisted bilayer graphene.

- Phys. Rev. B* **81**, 161405 (2010).
20. Miller, D.L. et al. Structural analysis of multilayer graphene via atomic moiré interferometry. *Phys. Rev. B* **81**, 125427 (2010).
 21. Ando, T. & Uemura, Y. Theory of Oscillatory g Factor in an MOS Inversion Layer under Strong Magnetic Fields. *J. Phys. Soc. Jpn.* **37**, 1044-1052 (1974).
 22. Smith, A.P., MacDonald, A.H. & Gumbs, G. Quasiparticle effective mass and enhanced g factor for a two-dimensional electron gas at intermediate magnetic fields. *Phys. Rev. B* **45**, 8829 (1992).
 23. Dial, O.E., Ashoori, R.C., Pfeiffer, L.N. & West, K.W. High-resolution spectroscopy of two-dimensional electron systems. *Nature* **448**, 176-9 (2007).
 24. Zhang, C. & Joglekar, Y. Wigner crystal and bubble phases in graphene in the quantum Hall regime. *Physical Review B* **75**, 1-6 (2007).
 25. Wang, H., Sheng, D., Sheng, L. & Haldane, F. Broken-Symmetry States of Dirac Fermions in Graphene with a Partially Filled High Landau Level. *Physical Review Letters* **100**, 1-4 (2008).
 26. Rezayi, E., Haldane, F. & Yang, K. Charge-Density-Wave Ordering in Half-Filled High Landau Levels. *Physical Review Letters* **83**, 1219-1222 (1999).
 27. Lilly, M., Cooper, K., Eisenstein, J., Pfeiffer, L. & West, K. Evidence for an Anisotropic State of Two-Dimensional Electrons in High Landau Levels. *Physical Review Letters* **82**, 394-397 (1999).
 28. Nayak, C., Simon, S.H., Stern, A., Freedman, M. & Das Sarma, S. Non-Abelian anyons and topological quantum computation. *Rev. Mod. Phys.* **80**, 1083 (2008).
 29. Eisenstein, J.P. & MacDonald, A.H. Bose-Einstein condensation of excitons in bilayer electron systems. *Nature* **432**, 691-694 (2004).
 30. Berger, C. et al. Ultrathin Epitaxial Graphite: 2D Electron Gas Properties and a Route toward Graphene-based Nanoelectronics. *The Journal of Physical Chemistry B* **108**, 19912-19916 (2004).

Supplementary Information is linked to the online version of the paper at www.nature.com/nature.

Acknowledgements We thank N. Zhitenev for useful discussions, S. Blankenship, A. Band, and F. Hess for their technical contributions to the construction of the mK SPM system, V. Shvarts for his advice on cryogenics, and U. D. Ham for instructions on making Ag probe tips. This work was supported in part by: the Korea Research Foundation Grant funded by the Korean Government (MOEHRD) (KRF- 2006-214-C00022), the NSF (DMR-0820382 [MRSEC], DMR-0804908, DMR-0606489), the Welch Foundation, and the Semiconductor Research Corporation (NRI-INDEX program).

Author Contributions Y.J.S, A.F.O, Y.K., and J.A.S designed and constructed the mK SPM system. The graphene STM/STS measurements were performed by Y.J.S, A.F.O, and J.A.S. The graphene sample was grown by Y.H and W.A. dH, and the surface prepared/characterized by D.B.T and P.N.F. A

theoretical analysis of the epitaxial graphene multilayer system was performed by H.M., S.A., M.D.S, and A.H.M.

Author Information The authors declare no competing financial interests. Correspondence and requests for materials should be addressed to J.A.S. (joseph.stroscio@nist.gov).

Figure Legends

Figure 1: Landau level spectroscopy of epitaxial graphene on SiC. Tunnelling spectroscopy of the Landau level states in the differential conductivity vs. sample bias. Tunnelling parameters: setpoint current 400 pA, sample bias -300 mV, modulation voltage 1 mV. (upper left inset) High resolution STM image of the graphene honeycomb lattice. Tunnelling parameters: setpoint current 100 pA, sample bias -250 mV, T=13 mK. (upper right inset) Landau level peak energy position (referenced to the $N=0$ level) vs. the square root of the Landau index, N , and magnetic field, B . Excellent scaling is observed in the linear relationship, yielding a carrier velocity of $(1.08 \pm 0.03) \times 10^6$ ms $^{-1}$ (1σ).

Figure 2: Landau levels of epitaxial graphene on SiC as a function of magnetic field. A series of dI/dV line scans, taken vertically through the moiré region in Supplementary Fig. 1, as a function of magnetic field. Each panel shows the dI/dV intensity in a colour scale (from -1 nS to 12 nS) with the horizontal axis as the sample bias, and the vertical axis within each panel is the distance 0 nm to 40 nm. A splitting of the $N=0$, 1, and 2 Landau levels can be seen in different field ranges. Tunnelling parameters: setpoint current 200 pA, sample bias -250 mV, modulation voltage 250 μ V, T=13 mK.

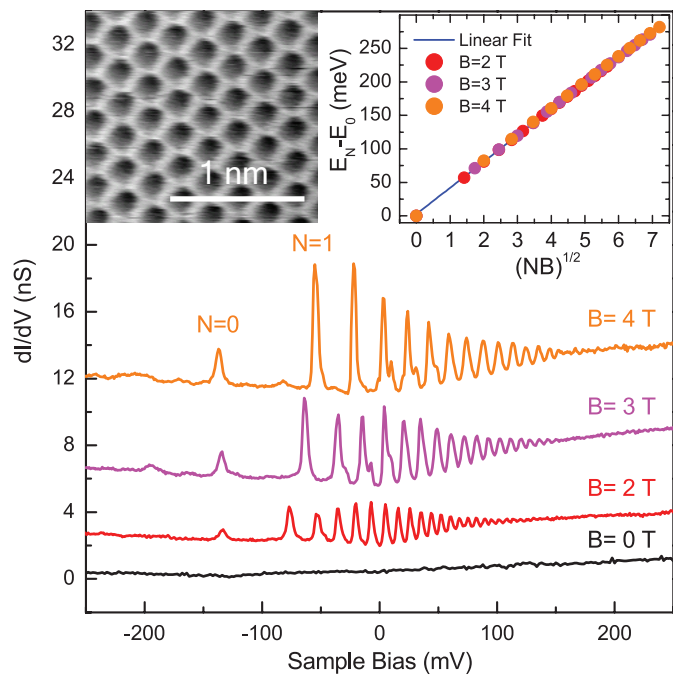
Figure 3: Electron density and filling factor variation with magnetic field of epitaxial graphene. (a) The electron density, $n=vB/\Phi_0$, determined from the filling of the Landau levels (red symbols), as a function of magnetic field B ,

where v is the filling factor and Φ_0 is the flux quantum. The dashed blue lines correspond to densities at constant filling factors ranging from $v=3$ to $v=14$. (b) The integral of the dI/dV spectra of the filled K' valley (from the middle of the $N=1$ LL to zero sample bias, E_F) as a function of field (see Fig. 4). The plateaus correspond to stable filling factors. (c) Electron density vs B in the region around 11.5 T showing the transitions between the 1/2-filled states at $v=9/2$ and $v=11/2$ between $v=4$ to $v=5$, and $v=5$ to $v=6$, respectively. Filling factors were determined by taking the ratio of the integrated areas in (b) and dividing by the area of a single LL (area at $v=5$) and adding 4 (2 for $N=0$ and 2 for K valley). The calculated filling factors are: 5.46 ± 0.06 , 4.54 ± 0.04 , and 3.52 ± 0.05 (1σ).

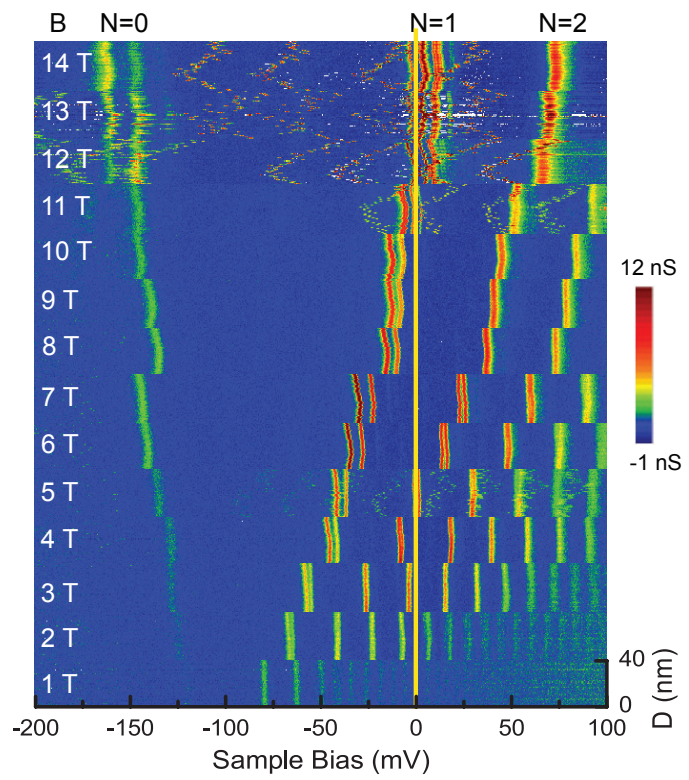
Figure 4: High resolution Landau level spectroscopy of the four-fold states that make up the $N=1$ LL. (a) A series of dI/dV line scans focusing on the Fermi-level region of the $N=1$ LL, taken in the same spatial location as in Fig. 2. At 11.125 T and 11.5 T a new stable 1/2-filled LL appears at filling factors of 11/2 and 9/2. (b) Single dI/dV spectra from the middle regions of the panels in (a) for the indicated magnetic fields. The level separation energies are defined in the various panels. ΔE_V , the lifting of the valley degeneracy (blue and red lines), is measured from the centres of the two spin split states (see 11.75 T). We define three energy separations for the spin split peaks, ΔE_{SL} and ΔE_{SR} for the left and right spin split levels, respectively (see 11 T); ΔE_{SE} measures the enhanced spin splitting when the Fermi-level falls in-between the spin split levels (see 11.25 T), and ΔE_{SF} measures the separation between the two 1/2-filled LLs. Tunnelling parameters: setpoint current 200 pA, sample bias -250 mV, modulation voltage 50 μ V, $T=13$ mK.

Figure 5: Energies in the epitaxial graphene $N=1$ Landau level. (a) Valley splitting, ΔE_V , measured for the $N=1$ Landau level as a function of magnetic

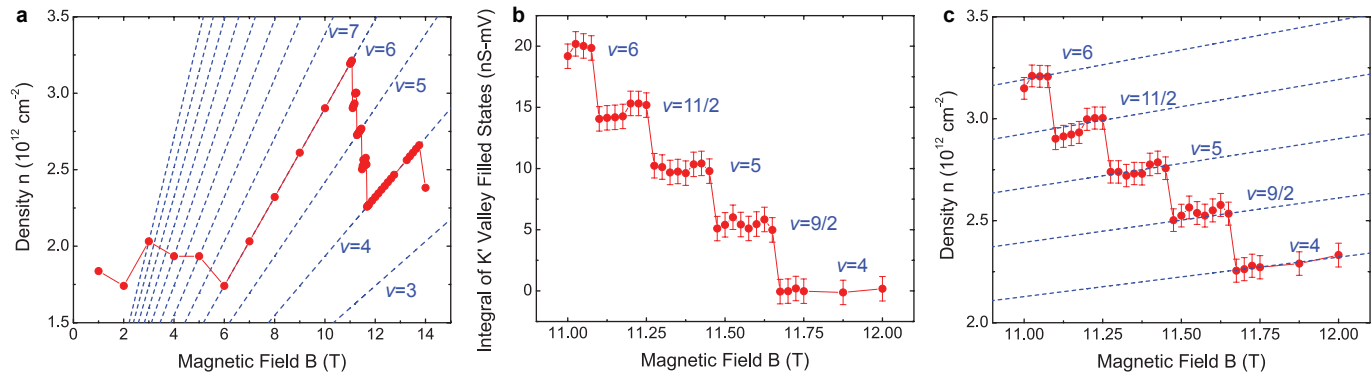
field. The solid blue line is a linear fit of the $N=1$ data for fields less than 7 T. The linear fit yield effective g -factors; $g_V(LL_1) = 18.4 \pm 0.4$ (1σ). The smooth cyan line is a guide to the eye and shows the $N=1$ splitting peaking when E_F is centred in the $N=1$ Landau manifold at a filling factor of 4. (Upper inset)
Schematic of the energy level structure of the $N=1$ LL showing the breaking of the valley symmetry, ΔE_V , followed by the breaking of the spin symmetry, ΔE_S .
(b) Spin-level energy separations as a function of magnetic field. The solid lines are linear fits yielding g -factors; $g_{SL}=2.36 \pm 0.01$, $g_{SR}=2.23 \pm 0.01$ (1σ). The level separation energies are defined in Fig. 4.



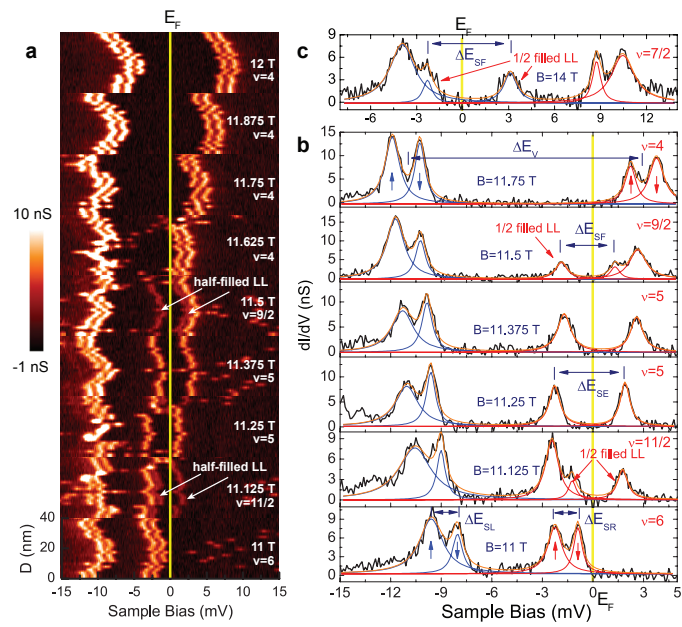
Stroscio Figure 1, print color full single column 89 mm wide.



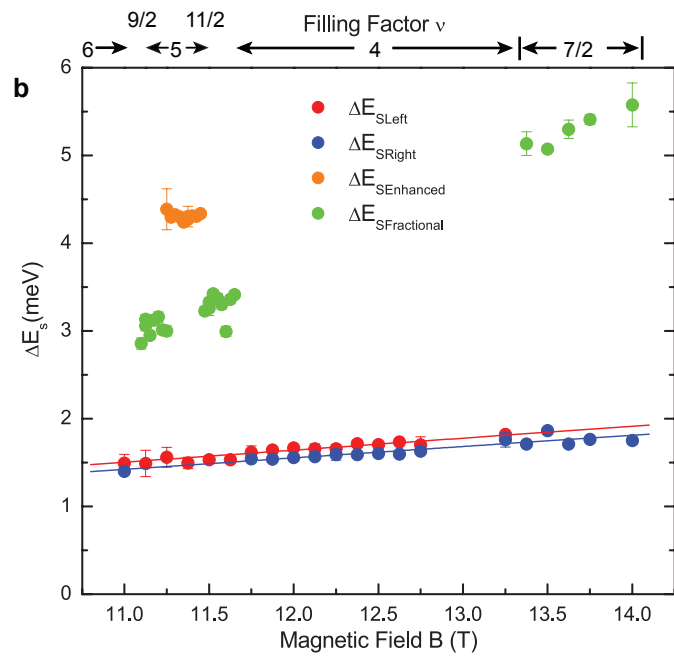
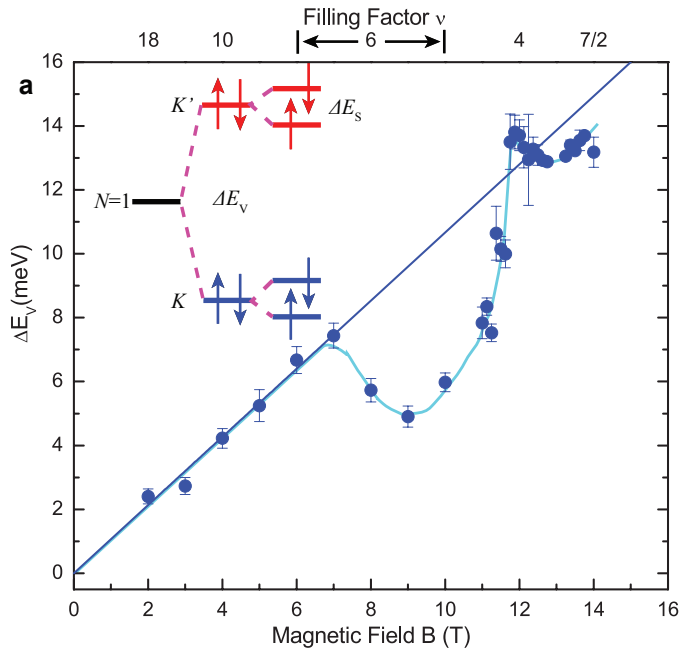
Stroscio Figure 2, print color full single column 89 mm wide.



Stroscio Figure 3 print colour full two columns 183 mm wide



Stroscio Figure 4 print colour full single column 89 mm wide



Stroscio Figure 5, print color full single column 89 mm wide.